Defect formation and migration in Nasicon $Li_{1+x}Al_xTi_{2-x}(PO_4)_3$

Hamid R. Arjmandi[a] , Steffen Grieshammer[a,b,c,*]

[a]*Institute of Physical Chemistry, RWTH Aachen University, Landoltweg 2, 52056 Aachen, Germany.*

[b]*Helmholtz-Institut Münster (IEK-12), Forschungszentrum Jülich GmbH, Corrensstr. 46, 48149 Münster, Germany.*

[c]*JARA-HPC, Forschungszentrum Jülich, RWTH Aachen University, Germany.*

Abstract

NASICON-structured materials of the composition $Li_{1+x}Al_xTi_{2-x}(PO_4)_3$ are regarded as solid electrolytes with high Li-ion conductivity applicable in all solid-state batteries. In this study we investigate the migration paths of constituting ions and monovalent charge carriers including K^+, Na^+, and, H^+. The results proof that Li is the most mobile species in the investigated composition and that the formation of intrinsic defects is unlikely. In addition, we find surprisingly low migration energy for oxygen vacancies in the structure of the dedicated Li-ion conductor.

1. Introduction

Energy storage is a key challenge in the transition from fossil fuels to renewable sources and the shift towards a sustainable energy future. In addition, many electronic devices, such as cellphones, laptops, and electric vehicles, require batteries with high energy densities. All solid state lithium ion batteries have recently attracted growing interest due to safety concerns and possibly higher energy densities compared to state-of-the-art lithium ion batteries with liquid electrolytes.

Several solid state Li-ion electrolytes are known with NASICON type materials showing high ionic conductivity at low material cost. Among these structures, Al-doped $LiTi_2(PO_4)_3$ (LATP) shows the highest conductivity.[1]

NASICON-structured materials crystallize in the space group $R\bar{3}c$.[2–5] The unit cell consists of Li on 6b, Ti on 12c, P on 18e, and two oxygen atom positions O1 and O2, both on 36f lattice sites. The rhombohedral structure contains a three-dimensional flexible framework with corner sharing TiO_6 octahedra and PO_4 tetrahedra. Aside from the introduced 6b position for Li (labeled as M1), there is another possible position for lithium occupation (M2). This site lies between two M1 sites at Wyckoff position 18e, surrounded by eight oxygen atoms with three times the multiplicity of the M1 position. The more stable M1 position is located between two TiO_6 octahedra, surrounded by six oxygen atoms. Li can also be displaced to M1/2 sites (Wyckoff position 36f), which is located between M1 and M2 sites.[5,6]

In the past few years, various experimental studies have been dedicated to the conductivity of Li-NASICON materials. A comprehensive review of conductivity and activation energy values for Li-NASICON structures can be found in the literature.[1] For $Li_{1+x}Al_xTi_{2-x}(PO_4)_3$ the highest total ionic conductivity is found for x around 0.3 with values of around 1.3×10^{-3} S·cm^{-1} for samples prepared by either solid-state reaction or sol-gel method and bulk conductivity is up to 5×10^{-3} S·cm^{-1}.[7]

^{7}Li-NMR measurements have been applied to investigate the structure and conduction mechanism in undoped LTP.[8,9] París et al. reported a preference of lithium to occupy the octahedral M1 sites of the structure and an energy barrier of 0.47 eV for Li-ion conduction. They also claimed that besides lithium mobility, the occupation of the M2 sites increases as well with increasing temperature. Arbi et al. reported a conductivity of 1.6×10^{-6} S·cm^{-1} and an activation energy of 0.46 ± 0.04 eV.

Ab-initio calculations based on density functional theory (DFT) allow the investigation of migration mechanisms on an atomic scale and represent the basis for multi-scale modeling of battery materials as a guide for future developments. [10]

have been performed to elucidate the conduction mechanism in LATP. Lu et al.[11] reported the lowest energy barrier for vacancy diffusion in LTP to be 0.42 eV, while the lowest barrier for interstitial diffusion was reported to be 0.25 eV. Similar results were reported by Lang et al.[12] for LTP with energy values of 0.41 eV and 0.19 eV, respectively.

Recently, alternative charge carriers for Li^+ such as Na^+ have attracted interest to decrease cost and realize new cell chemistries. In addition, the influence of water on the ionic conductivity has been discussed recently.[13,14] As the electrochemical stability window is limited, reactions at the interface with the electrodes are not thermodynamically but kinetically hindered. Therefore, the concentration and mobility of intrinsic defects could play a crucial role for the long term stability of the material.

In this paper, we therefore, investigate defect formation and migration for the constituting ions Ti^{4+}, O^{2-}, and P^{5+}, and examine the incorporation and migration of the monovalent ions H^+, Na^+, and K^+ using DFT.

2. Computational Details

Spin-polarized DFT+U calculations were performed with the program VASP[15] applying the generalized-gradient approximation (GGA) functional by Perdew-Burke-Ernzerhof revised for solids (PBEsol)[16] and the projector augmented-wave method (PAW).[17] A Hubbard-type correction in the simplified rotationally-invariant scheme[17,18] was included with a value of *U*=2.50 eV for the *d*-electrons of Ti as suggested by Lu et al.[11] A cut-off energy for plane waves of 500 eV was used for the determination of the lattice constants and the band gap and of 400 eV for defect calculations. Further test calculations with a cut-off of 500 eV revealed no significant difference for energies of formation and migration. The convergence criterion for energy and forces were set to 10^{-4} eV and 0.01 eV/Å for electronic relaxation and ionic relaxation, respectively. The configurations *Li* $1s^2 2s^1$, *Ti* $3s^2 3p^6 4s^2 3d^2$, *P* $3s^2 3p^3$, *O* $2s^2 2p^4$, *Na* $2p^6 3s^1$, *Al* $3s^2 3p^1$, *K* $3s^2 3p^6 4s^1$, and *H* $1s^1$ were treated as valence electrons.

For the calculation of defect formation and migration a supercell containing eight formula units was generated from the primitive cell with the transformation matrix of [1, 1, -1; -1, 1, 1; 1, -1, 1] as suggested by Lu et al.[11] (Figure 1). A Γ-centered 2 × 2 × 2 k-point mesh was applied.

For charged defects, the charge was either compensated by oppositely charged defects or by a homogeneous background charge that is automatically introduced in VASP. The migration pathways

were explored using the climbing image nudged elastic band (CI-NEB) method[19] with three intermediate images for each migration step.

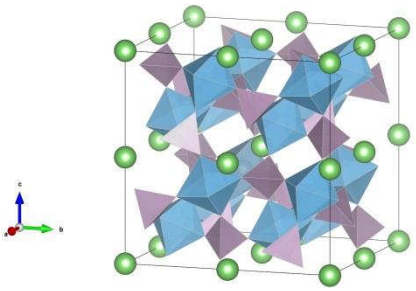

Figure 1: Visualization of LTP supercell. Blue octahedra and purple tetrahedra represent TiO_6 and PO_4 units, respectively. Lithium ions are shown in green at the M1 positions.

3. Results and Discussion

3.1 Bulk properties

The lattice parameter of the pure LTP cell was derived by fitting the Birch-Murnaghan equation of state,[20] resulting in a bulk modulus of 89.4 GPa and a lattice constant of 8.55 Å for the primitive cell. The calculated lattice constant has been significantly improved in comparison to the value of 8.68 Å obtained from the PBE functional,[11] which is farther from the experimental value of 8.51 Å.[2–5] This lattice constant was fixed for all subsequent calculations. The band gap of LTP is overestimated with 2.5 eV compared to the experimental value of 2.10 eV[21] as has been reported before.

3.2 Aluminum Doping

Al-doped cells of $Li_{1+x}Al_xTi_{2-x}(PO_4)$ with x=0.125 and 0.25 were created, corresponding to 1 and 2 Al-ions in the supercell, respectively. Each aluminum ion is charge compensated by one additional Li-ion.

The additional Li-ions are placed at sites suggested from previous experimental and computational results.[11,12,22–24] The introduction of additional lithium perturbs the adjacent regular Li position at the M1 site to reduce electrostatic repulsion pushing it slightly away to a new energetically favorable site, such that both additional and regular ions occupy equivalent M1/2 sites. This finding is in agreement with the previous calculations by Lang et al.[12] and Lu et al.[11] as well as the neutron diffraction and NMR study by Arbi et al.[23] However, in the case where one Li-ion occupies M2 the total energy of the cell is only 0.01 eV higher, suggesting stable positions at both the M1/2 and M2 site.

Various configurations for the locations of Al and additional Li are possible and were explored for the case of x=0.125. It was found that Al is prone to be situated as close as possible to the interstitial Li couple due to the opposite relative charges of $Li_i^{\cdot}$ and $Al_{Ti}^{/}$. Here the Li-couple is tilted toward Al, such that one Li-ion is placed closer to Al (Figure 2). The other calculated configurations have energies of 0.07 eV to 1.18 eV relative to the most stable configuration without any notable trend regarding the $Li_i^{\cdot} - Al_{Ti}^{/}$ distance.

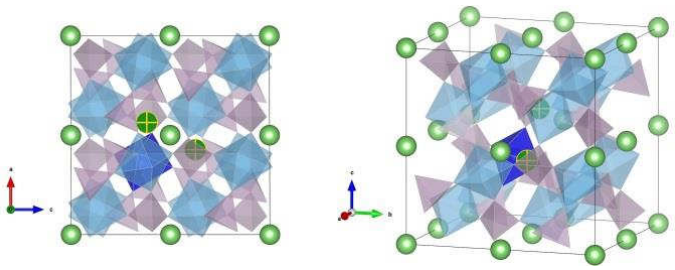

Figure 2: The most stable LATP supercell with Al concentration of 0.125. The crossed dark green ions represent the interstitial Li couple and the dark blue octahedron belongs to the Al-ion.

For the case of x=0.25 configurations were generated with the supercell program[25] and 20 configurations with the lowest electrostatic energy were optimized.

In the most stable configuration, the two Al-ions are located as distant as possible within the supercell with one interstitial Li couple close to one Al and the second couple placed between the two Al-ions (cf. Figures S1). In addition, there are several configurations with less than 0.01 eV higher energies.

3.3 Lithium Ion Migration

Vacancy migration and interstitial migration were investigated in LTP and LATP, respectively, using the CI-NEB method.

LTP

In the stoichiometric composition LTP no extrinsic but only intrinsic defects are present. For the case of vacancy migration Lu et al.[11] suggested the direct migration of a regular Li-ion to an adjacent vacant M1 site through a M2 site with a distance of 6.12 Å (cf. Figure S2). Here, the transition state corresponds to the M2 position in contrast to the interstitial case where this is another stable Li positionOur calculated value of 0.48 eV agrees with the value of 0.42 eV by Lu et al. and the experimental value of 0.48 ± 0.1 eV.[9] Nevertheless, the comparison with experiment should be treated cautiously as for nominally pure LTP the origin of defects and the prevailing migration mechanism is not clear. We therefore calculated the energy of Frenkel disorder for lithium in LTP with a value of 0.64 eV. Although this value is comparatively small, the amount of intrinsic defects at room temperature will be in the ppm range and deviations from stoichiometry in the synthesis process are possibly the major source of defects.

LATP

The introduction of additional Li-ions through Al-doping leads to conduction by Li-interstitials. We calculated possible migration pathways in the most stable cell with x=0.125. This doping concentration is lower than the typical experimental value but allows the detailed study of the effect of individual dopant ions on the migration energies. The most favorable pathway is the migration of a Li-ion from M1/2 site of a Li-interstitial-couple through a M2 site to a new M1/2 site, thereby pushing

another regular Li-ion from its M1 site to a M1/2 site while other Li-ion of the original couple relaxes to its M1 site. Two different paths of this type along (0,1,0) were calculated by CI-NEB; one with the Al along the path (path 1) and one without the Al along the path (path 2). Additionally, two farther paths along (1,0,-1) (path3) and (1,1,-1) (path 4) were calculated for comparison. The resulting energy profiles are depicted in Figure 3 and migration energies and distances are given in Table 1. The migration paths are illustrated in the supporting information (Figure S3).

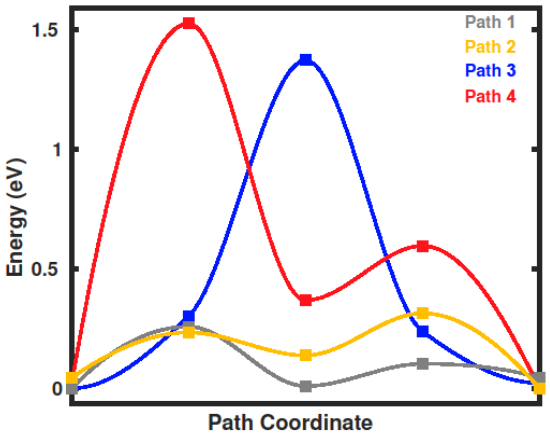

Figure 3: Energy profiles for various possible pathways in different colors for interstitial Li migration in LATP with x=0.125.

It should be mentioned that all stable positions within the supercell for Li occupation were covered as initial and final states in Li migration. Moreover, further possible positions turned out to be unstable and ended up with the previously studied configurations.

Table 1: Li migration length and energies of the pathways shown in Figure 3.

	Li migration length (Å)	Energy barrier (eV)
Path 1	6.07	0.26
Path 2	6.14	0.31
Path 3	8.34	1.37
Path 4	10.45	1.52

Combination of paths 1 and 2 allows the migration through the complete cell (cf. Figure S4). The corresponding energy profile is given in Figure 4. Here, sites *a* and *i* are identical and site *e* is the M1/2 position farther from the Al-ion with a relative energy of 0.03 eV. The energy profile not only reflects the favorable positioning of the Li interstitial close to Al but also that the migration barrier is increased close to the Al-ion.

Based on experimental results, Martinez et al.[24] suggested that the additional Li-ions occupy M2 sites while calculations of Lu et al.[11] and Lang et al. [12] claimed the M1/2 site to be preferred. The latter conclusion was also drawn by Arbi et al.[22] based on neutron diffraction. The calculations here show that the M1/2 site is indeed favorable but the M2 site is only slightly higher in energy, depending on its position relative to Al.

In literature, the migration energy is often rationalized in terms of a bottleneck, reflecting the narrowest section along the path. The distance to the adjacent oxygen ions, the volume of the

formed LiO_4 tetrahedron, the distance to the nearest cation, and the traveled distance of the migrating Li-ion were calculated for the reported pathways (cf. Table. S1). The peek energy of each path indicates that as the cation or anion bottleneck shrinks, the energy barrier increases. Additionally, it was found that the migration length of the migrating ion could be a fair indicator for the most favorable path. The data for the most favorable path, i.e. path 1 in Figure 3, shows that although the energy is raised with an increase of the average distance between Li and the adjacent oxygen and the volume of the tetrahedron, the trend is reverse for the distance of Li to the nearest cation or anion (cf. Table. S2).

A similar path through the cell with x=0.25 was calculated with a total barrier of 0.21 eV. These values are in agreement with the measured bulk activation energies where the energy decreases with increasing Li content.[1] The reason for this behavior is not clarified but it is likely that a higher Al content leads to a more homogeneous energy landscape, leading to a reduction of the total barrier. At low Al-content the Li interstitials get trapped at the Al-ions due to the energetic preference of these configurations as discussed above (compare states g, h and i in Figure 4). The individual steps of the calculated path for x=0.25 start and end at an Al-ion thus there is no trapping effect and the effective migration barrier is lower.

High ionic conductivity in solid conductors can be achieved through a combination of high charge carrier concentration and low migration barriers. The ionic conductivity in the structure can be calculated with the migration barrier E_{mig} and the attempt frequency ν_0 by

$$\sigma = \frac{cq^2}{k_B T}\frac{Z}{6} l^2 \nu_0 \exp\left(-\frac{E_{\mathrm{mig}}}{k_{\mathrm{B}} T}\right)$$

where c, q, l and Z are the concentration of mobile charge carriers, their charge, the jump distance and the number of jump directions, respectively. Here we approximate ν_0 with a typical value of 10^{13} Hz and for x=0.125 and x=0.25 we obtain values of 7×10^{-4} S·cm^{-1} and 7×10^{-2} S·cm^{-1}, respectively. It is noted that the calculated conductivities are sensitive to the exact value of E_{mig} and that the exact value of ν_0 is not known. Nevertheless, the reported bulk conductivities of about $5\cdot10^{-3}$ S/cm are within the calculated range.

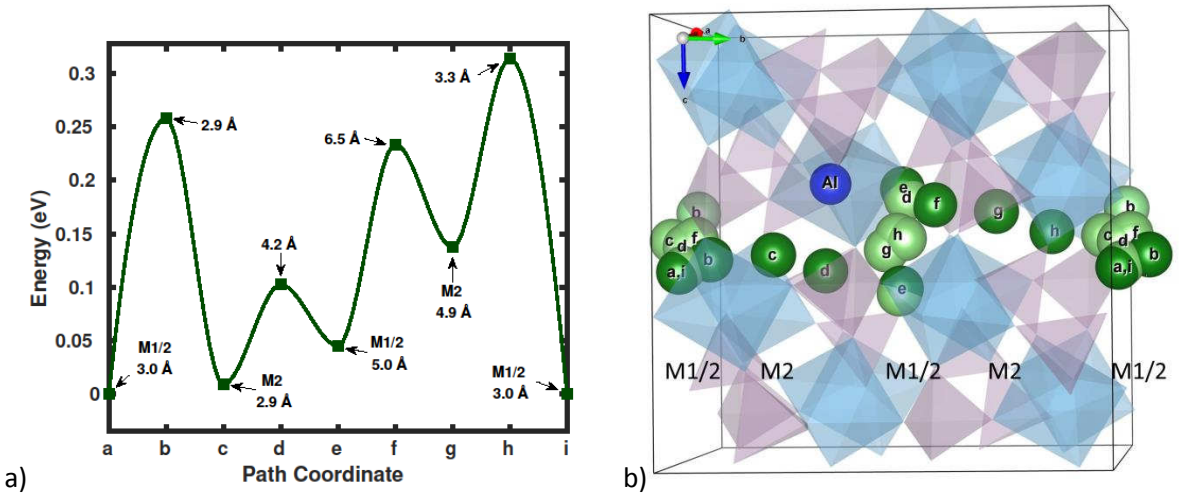

Figure 4: a) Energy profile of the most favorable path (combination of paths 1 and 2) for interstitial Li migration in LATP here x=0.125. The distance between Al and migrating Li is labeled in Å for each step. b) corresponding visualization of the migration path. Labels correspond to labels in a)

3.4 Intrinsic defects

Defect formation

The energy of formation ΔE_{Fr} of intrinsic defects due to Frenkel disorder was calculated for O, Ti, and P according to

$$\Delta E_{Fr} = E_{Frenkel} - E_{bulk}, \qquad (1)$$

where $E_{Frenkel}$ and E_{bulk} are the energies of the defective cell and the bulk cell, respectively. In principle, the energy could be calculated from the isolated defects in charged supercells. However, this introduces an unphysical interaction of the charged defect with its images in the periodic cells as well as with the compensating background charge. Therefore, we included both defects in one neutral supercell with the largest possible separation within the periodic cell. We note that there is still interaction between the defects within the cell and between the cells, which implies a very high defect concentration. Since the oppositely charged defects are expected to stabilize each other, the calculated values must be regarded as a lower bound for the formation energy.

Calculations were performed for LTP and the most stable configuration of $Li_{1.125}Al_{0.125}Ti_{1.875}(PO_4)$ with different defect positions relative to Al-ion in the latter case. The lowest energy for each case is given in Table 2.

Table 2: Energies of defect formation for Frenkel defects in LTP and LATP given in eV.

Defect pair	LTP	LATP
$Ti_i^{4\cdot} - V_{Ti}^{4/}$	15.6	11.5
$P_i^{5\cdot} - V_P^{5/}$	10.0	8.7
$O_i^{//} - V_O^{\cdot\cdot}$	15.4	6.4

It is worth noting that the most stable LATP structure with a Ti or a P vacancy is obtained when the respective vacancy was created next to Al. In this case, the adjacent Li ion moved to the vacant site forming $Li_{Ti}^{3/}$ or $Li_P^{4/}$. This could explain the large differences of Frenkel energies between LTP and LATP.

Defect migration

Migration paths for vacancies and interstitials were calculated for LTP for the most stable configurations. For each case the four shortest migration paths were considered. The profiles with the lowest energies for interstitial and vacancy migration are depicted in Figure 5 and 6, respectively and migration paths are illustrated in the supporting information. It should be noted that due to the symmetry, only the first half of the path through the cell is shown. While the cationic defects $P_i^{5\cdot}$ and $Ti_i^{4\cdot}$ have similar barriers with 1.13 eV and 1.45 eV, respectively, the barrier for the oxygen interstitial is considerably higher with 3.74 eV.

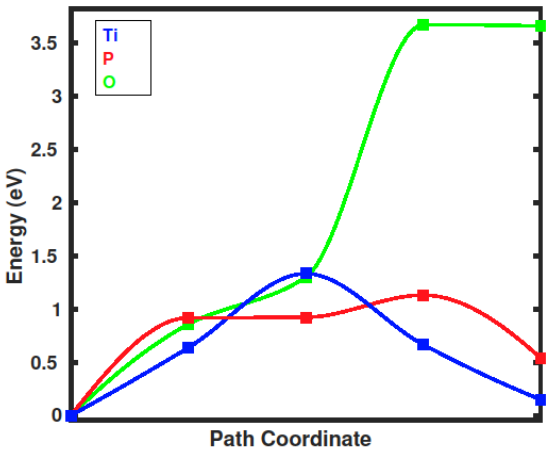

Figure 5: Migration energy profile for interstitial Ti, P, and O in LTP.

In contrast, the energy profiles for vacancy migration show higher migration energies of 2.81 eV and 4.31 eV for $V_{Ti}^{4/}$ and $V_{P}^{5/}$ than for the oxygen vacancy with 0.45 eV. The results can be summarized in that defects with relative positive charge, i.e. cation interstitials and oxygen vacancy, exhibit lower barriers than defects with relative negative charge, i.e. cation vacancies and oxygen interstitial.

While most migration energies except for Li are well above 1 eV, the barrier for oxygen vacancies is just 0.45 eV. This is a surprisingly low value when considering the migration barrier of about 0.5 eV in the oxygen ion conductor cerium oxide. However, the concentration of oxygen vacancies is expected to be low due to the high energies of defect formation and therefore only vacancies due to deviations in the synthesized stoichiometry are reasonable. With an oxygen vacancy site fraction of 10^{-3} we calculate a conductivity of 6×10^{-8} S·cm^{-1}.

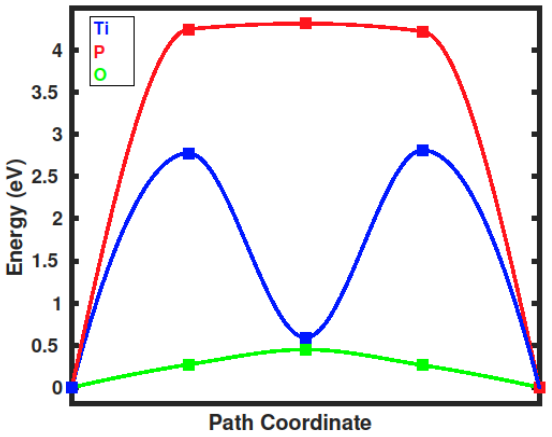

Figure 6: Migration energy profile for Ti, P, and O vacancy in LTP.

3.5 Other charge carriers

We examined the migration of other monovalent ions, namely Na^+ and K^+ in the LATP structure. The interstitial Li-ion was thus replaced by a Na- or K-ion in the most stable configurations of LATP with x=0.125 and the migration paths corresponding to path 1 and path 2 were calculated (cf. Figure S7 and S8).

It appears that the Na case not only ended up with the same ions arrangement as LATP, but also their most favorable conduction pathways are the same. As demonstrated in Figure 7, the energy barrier for the Na-ion transport is calculated to be 0.69 eV, with one fewer local minimum compared to the Li migration energy profile, which is also supported by Lu et al.[11] It should be noted that the position of ions in each step of migration is similar to LATP with one additional Li-ion.

For potassium, the calculation results indicate that the K-ion would rather occupy the M1 position than the M1/2 site. In fact, the introduced K pushes away the Li-ion to an M2 site and K takes over the regular Li site. It might be worth mentioning that the reverse arrangement with Li on M1 and K on M2 has a 0.17 eV higher energy. However, the structure with a K-ion ended up with a similar migration pathway as Li in LATP. Figure 7 represents the pathway energies for K migration with an M1-M1/2-M1 pathway, yielding the value of 1.05 eV as the highest barrier.

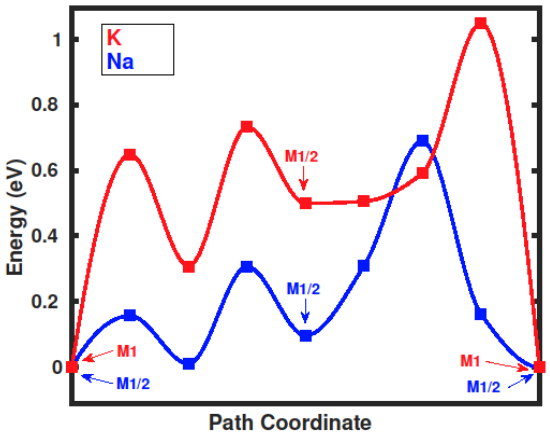

Figure 7: Migration energy profile for Na- and K-ion with M1/2-M1/2-M1/2 and M1-M1/2-M1 migration routes, respectively.

In addition we calculated corresponding migration paths for the fully substituted compositions NATP and KATP, where all Li –ions are replaced by Na-ions or K-ions, respectively. The migration paths and energies are comparable with the calculations of the singly substituted compositions with highest barriers of 0.82 eV and 1.24 eV for NATP and KATP, respectively. (cf. Figure S9 for the energy profiles.)

The previous results suggest that the energy increases with increasing size of the migrating cation. Therefore, a fast migration of protons in the lattice could be expected. Indeed, experimental results suggest that exposure to moist atmosphere could increase the electrical conductivity of LATP, although the reported literature is not consistent.[13,14]

We investigated two possibilities of incorporation of protons in the lattice. On the one hand, water can be incorporated into the structure at the expense of oxygen vacancies or accompanied by the formation of oxygen interstitials.

$$\mathrm{H_2O} \rightarrow \mathrm{O_i^{//}} + 2\mathrm{H_i^{\cdot}} \qquad (2)$$

$$\mathrm{H_2O} + \mathrm{V_O^{\cdot\cdot}} \rightarrow \mathrm{O_O^{\times}} + 2\mathrm{H_i^{\cdot}} \qquad (3)$$

Note that eqs. (2) and (3) are related by anti-Frenkel disorder. We calculated the energy of hydration for eq. (2) from

$$E_{\mathrm{hydration}} = E\left(\mathrm{O_i^{//}}, 2\mathrm{H_i^{\cdot}}\right) - E(\mathrm{H_2O}) - E(LTP) \qquad (4)$$

Where $E\left(\mathrm{O_i^{//}}, 2\mathrm{H_i^{\cdot}}\right)$ is the energy of a cell with an oxygen interstitial and two protons and $E(\mathrm{H_2O})$ and $E(LTP)$ are the energies of the water molecule and a bulk LTP cell, respectively. This calculation leads to an energy of hydration of 3.6 eV. The energy for eq. (3) is calculated from this value by subtracting the energy of anti-Frenkel disorder resulting in a value of -11.8 eV. Consequently, the hydration of the lattice is likely but only if oxygen vacancies already exist.

On the other hand, protons can be incorporated by direct exchange with Li-ions. The corresponding protonation energy is calculated by

$$E_{\mathrm{protonation}} = E(LHTP) + E(Li^+) - E(LTP) - E(H^+) \qquad (5)$$

with the energy of the proton containing cell $E(LHTP)$ and the energies of the free Li-ion and proton $E(Li^+)$ and $E(H^+)$, respectively. Here, $E(H^+)$ is set to zero as the H^+ contains no electron. The calculated value is 4.8 eV for LTP and between 4.0 eV and 4.4 eV for LATP depending on the position of proton. The exchange of Li-ions by protons in the bulk seems to be unfavorable. It should be noted that solvation effects of the ions may play a crucial role and also the energetics near the surface or at grain boundaries could be different, however, this is beyond the scope of the present study.

The migration of the proton through the cell was investigated and it was found that protons travel through a path with several locally stable arrangements of ions, where in these stable configurations, the proton is situated close to an O-ion (less than 1.4 Å). Consequently, the protons do not migrate through the middle of the largest bottleneck but along the oxygen ions of the polyhedral network in a combination of rotational jumps around one oxygen ion and translational jumps between neighboring oxygen ions(cf. Figure S10). The corresponding energy profile is depicted in Fig. 8 showing an energy barrier of 0.81 eV.

The energy of migration increases in the order Li < Na < H < K. This phenomenon indicates that smaller and lighter ions are usually more mobile except for H, which is not prone to being separated from surrounding O-ions due to the strong oxygen-hydrogen bond.

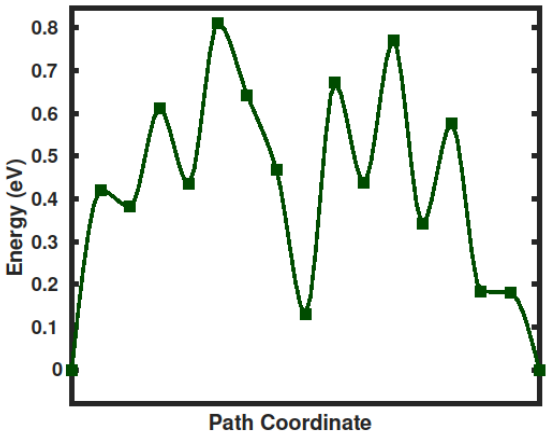

Figure 8: Migration energy profile for a proton.

Conclusion

We investigated the most stable configurations of $Li_{1+x}Al_xTi_{2-x}(PO_4)_3$ with x=0.125 and x=0.25 and Li-ion migration within the structures by DFT+U. We found that doping Al causes the formation of interstitial Li couples near the Al-ion, where both Li-ions occupy the M1/2 site. Additionally, the M2 position was also found to be stable with an only slightly higher energy. Using CI-NEB, the energy barrier for Li-ion migration was calculated along with the exploration of their conduction pathway. The vacancy migration energy for LTP was calculated to be 0.48 eV.

The interstitial migration in LATP has a lower energy barrier that depends on the position relative to the Al dopant. The values for LATP with x=0.125 and 0.25 are calculated to be 0.31 eV and 0.21 eV, respectively. These values are fully supported by experimental measurements. For sodium and potassium ions, higher migration energies were found where a larger ionic radius leads to a higher barrier. Nevertheless, for the migration of protons, a high energy barrier is found as well and the incorporation of protons in the bulk is unlikely unless oxygen vacancies exist in the lattice. We calculated the energies of Frenkel and anti-Frenkel disorder, finding that the formation of defects is unlikely. For the constituting ions P, Ti, and O in LTP, energy barriers of 1.13 eV, 1.45 eV, and 3.74 eV for interstitials and 2.81 eV, 4.31 eV, and 0.45 eV for vacancies were found, respectively. The results imply that positive defects have a smaller migration energy barrier compared to the negative defects of the same ion in this material and for the oxygen vacancy a surprisingly small value is found.

Acknowledgment

The authors gratefully acknowledge the computing time granted by the JARA-HPC Vergabegremium and provided on the JARA-HPC Partition part of the supercomputer CLAIX at RWTH Aachen University. Simulations were performed with computing resources granted by RWTH Aachen University under project rwth0256. The visualizations of the structures were generated with VESTA.[26]

ReferencesReferences

1 A. Rossbach, F. Tietz and S. Grieshammer, *J. Power Sources*, 2018, **391**, 1–9.

2 N. Bounar et al., *Physica B: Condens. Matter*, 2012, **407**, 403–407.

3 E. Dashjav and F. Tietz, *Z. anorg. allg. Chem.*, 2014, **640**, 3070–3073.

4 A. Aatiq et al., *J. Mater. Chem.*, 2002, **12**, 2971–2978.

5 I. Pinus et al., *Solid State Ionics*, 2012, **212**, 112–116.

6 a) K. Arbi, M. Ayadi-Trabelsi and J. Sanz, *J. Mater. Chem.*, 2002, **12**, 2985–2990; b) M. Catti, A. Comotti and S. Di Blas, *Chem. Mater.*, 2003, **15**, 1628–1632; c) A. Martínez-Juárez, J. E. Iglesias and J. Rojo, *Solid State Ionics*, 1996, **91**, 295–301;

7 a) M. Su et al., *Zhongguo Youse Jinshu Xuebao*, 2013, **23**, 469–473; b) H. Aono, *J. Electrochem. Soc.*, 1990, **137**, 1023; c) D. Rettenwander et al., *J. Mater. Chem. A*, 2016, **4**, 1506–1513;

8 K. Arbi et al., *Chem. Mater.*, 2002, **14**, 1091–1097.

9 M. A. París et al., *J. Phys.: Condens. Matter*, 1996, **8**, 5355–5366.

10 a) A. Urban, D.-H. Seo and G. Ceder, *Npj Comput. Mater.*, 2016, **2**, 16002; b) S. Shi et al., *Chinese Physics B*, 2016, **25**, 18212;

11 X. Lu et al., *Nano Energy*, 2017, **41**, 626–633.

12 B. Lang, B. Ziebarth and C. Elsässer, *Chem. Mater.*, 2015, **27**, 5040–5048.

13 E. Dashjav et al., *Solid State Ionics*, 2018, **321**, 83–90.

14 P. Zhang et al., *Solid State Ionics*, 2015, **272**, 101–106.

15 a) Kresse and Furthmüller, *Phys. Rev. B*, 1996, **54**, 11169–11186; b) G. Kresse and D. Joubert, *Phys. Rev. B*, 1999, **59**, 1758–1775;

16 J. P. Perdew et al., *Phys. Rev. Lett.*, 2008, **100**, 136406.

17 Blöchl, *Phys. Rev. B*, 1994, **50**, 17953–17979.

18 V. I. Anisimov, F. Aryasetiawan and A. I. Lichtenstein, *J. Phys.: Condens. Matter*, 1997, **9**, 767–808.

19 G. Henkelman, B. P. Uberuaga and H. Jónsson, *J. Chem. Phys.*, 2000, **113**, 9901–9904.

20 a) F. Birch, *Phys. Rev.*, 1947, **71**, 809–824; b) F. D. Murnaghan, *Proc. Nat. Acad. Sci. USA*, 1944, **30**, 244–247;

21 J.-Y. Luo and Y.-Y. Xia, *Adv. Funct. Mater.*, 2007, **17**, 3877–3884.

22 K. Arbi et al., *Inorg. Chem.*, 2013, **52**, 9290–9296.

23 K. Arbi et al., *Phys. Chem. Chem. Phys.*, 2014, **16**, 18397–18405.

24 A. Martínez-Juárez et al., *J. Phys. Chem. B*, 1998, **102**, 372–375.

25 K. Okhotnikov, T. Charpentier and S. Cadars, *J. Cheminf.*, 2016, **8**, 17.

26 K. Momma and F. Izumi, *J. Appl. Crystallogr.*, 2011, **44**, 1272–1276.